

Hyperelastic behavior of cellular structures based on micromechanical modeling at small strain

M. JANUS-MICHALSKA

*Institute of Structural Mechanics
Cracow University of Technology
Warszawska 24
31-155 Kraków, Poland
e-mail: mjm@limba.wil.pk.edu.pl*

THE PRESENT PAPER EXTENDS recent effective, linear anisotropic elasticity model [6, 7] for cellular materials by implying geometric nonlinearity, which is built as the constitutive relation between Green's Lagrangean strain in the tensor and the second Piola–Kirchhoff stress tensor and strain potential formulation. Cellular materials may easily experience large deformations due to large pores-to-volume ratio, since such a deformation on the macroscopic level usually requires smaller deformations of the individual struts constituting the skeleton. The formulation based on micromechanical modeling assumes that essential macroscopic features of mechanical behavior on a macro scale, can be inferred from the deformation response of a representative volume element. Open-cell materials with diverse regular skeleton structures are considered. The initial stiffness tensor components for anisotropic continuum are expressed as functions of microstructural parameters, such as skeleton geometric data of representative volume element and skeleton material properties. Since large strains in skeleton structure are characteristic for elasto-plastic behavior, interest is focused on the large displacement and small strain cases. Examples involving numerical tests on cellular materials under homogeneous strain, relevant to simple shearing and to uniaxial or biaxial loading in the tensile and compressive range, are considered.

Key words: cellular materials, anisotropy, effective model, micromechanical modeling, hyperelasticity, dissymmetry in tension-compression.

Copyright © 2011 by IPPT PAN

Notations

- E** Green–Lagrange strain tensor,
- A_i relative stretch along the i axis,
- Γ_{ij} change of angle between two perpendicular axes i, j ,
- F** deformation gradient,
- T** first Piola–Kirchhoff stress tensor,
- II** second Piola–Kirchhoff stress tensor.

Geometric microstructural parameters:

- \mathbf{b}_i^0 half strut of the length $|\mathbf{b}_i^0| = L_{0-i}/2$,
- L, h, t geometric microstructural parameters.

Material microstructural parameters:

- σ_f^s rupture modulus of skeleton material,
- E_s Young's modulus of skeleton material,
- β structure orientation angle,
- ${}^0\mathbf{S}$ initial stiffness matrix,
- λ_α eigenvalues of ${}^0\mathbf{S}$, $\alpha = \text{I, II, III}$,
- ${}^\alpha\tilde{\mathbf{E}}$ unit strain eigenstates,
- ${}^\alpha\mathbf{E}^{\text{cr}}$ critical strain eigenstates,
- k_α scalar multiplier for critical eigenstate,
- Φ_E strain energy density,
- ${}^\alpha\Phi_E^{\text{cr}}$ critical energy densities stored in eigenstates, $\alpha = \text{I, II, III}$.

1. Introduction

CELLULAR SOLIDS represent a class of materials investigated with increasing interest due to their unique properties. Macroscopic behavior described in terms of effective properties can be explained only by fundamental studies on a microscale. Such approach yields better understanding of overall properties and facilitates of the manufacture of custom-tailored materials. It is very important to correlate microstructural features with engineering design criteria in order to optimize manufacturing process and material selection. Generally, cellular materials are characterized by high deformability and reversibility of deformation due to their geometric structure of skeleton, thus showing hyperelastic behaviour. Large displacements on the macroscopic level usually result in smaller deformations of the individual struts constituting the skeleton. Nonlinear response of cellular material stems from reorientation of struts, originating in rigid motion of structural nodes. It is not necessary to invoke nonlinear behavior of the constituent material to predict nonlinear behaviour of cellular solid.

In this study, our interest is concentrated upon the geometric nonlinearity. Work is focused on the large displacement and small strain case. This is most typical for skeleton structure since for large strains, the elasto-plastic response in skeleton node areas should be taken into account. For compressive loads, struts buckling may occur. It is not accounted for in this analysis and limits the strains for which the model is valid.

The problem considered is not new, the geometrically nonlinear behaviour of cellulars was extensively studied by WARREN and KRAYNIK [1], WARREN, KRAYNIK and STONE [2] on the example of foam, using simplified pin-jointed model for which bending contribution for skeleton struts was neglected. Another approach was given by WANG and CUITIÑO [3] where axial, bending and twisting deformation at local level were considered. Both authors formulate the strain energy function. The latest study based on the homogenization technique was given by HOHE and BECKER [4].

Different models of microstructures are known in the literature. The most typical model is the truss model used by WARREN and KRAYNIK [1] and WARREN, KRAYNIK and STONE [2] and WANG and CUITIÑO [3], a very simplified model indeed. It assumes hinges associated with plastic deformation. This model works well only for stretching the dominant structures. Structures, in which stretching and simultaneous bending occurs, are analyzed on the basis of a beam model, which is successfully applied to linear analysis by JANUS-MICHALSKA and PEÇHERSKI [5] and JANUS-MICHALSKA [6].

The present study is a continuation of works on cellulars, based on micromechanical modeling by JANUS-MICHALSKA and PEÇHERSKI [5], JANUS-MICHALSKA [6], KORDZIKOWSKI, JANUS-MICHALSKA and PEÇHERSKI [7] and extends recent linear effective model. It is used to construct the strain-stress relation and strain energy function for the hyperelastic cellular material with arbitrary symmetry. The main advantage of such an approach is that the macroscopic constitutive model follows readily from the analytical or numerical treatment. The elastic stiffness and strength are expressed in terms of geometric and material parameters of a skeleton structure. Thus it is possible to prepare the material to special mechanical requirements. The effect of only geometrical nonlinearity for materials of different structures is analysed and the influence of microstructural parameters is studied. Significant differences between the infinitesimal strain behaviour and small strain regimes is observed.

2. Small strain anisotropic hyperelasticity

The basis of typical nonlinear analysis is a neo-Hookean constitutive relationship between Green's strain tensor and its conjugate stress, the second Piola–Kirchhoff stress tensor or formulation of the strain energy density. The purpose of this paper is to present a derivation of constitutive equation for the hyperelastic cellular material with arbitrary symmetry. The concept of multiscale modeling is applied to specify equivalent continuum as an effective model of cellular material by formulating appropriate constitutive equation on this level.

2.1. Strain and stress measures for nonlinear elasticity

The physical Green's Lagrangean strain tensor is formulated with respect to initial coordinate system. The material lines, which are orthogonal in the initial configuration, are considered to control deformations of the cellular continuum. Strain components that characterize the elongations of line elements parallel to the coordinate axes before deformation, are defined as follows [8, 9]:

$$(2.1) \quad E_{ii} = \frac{1}{2}(A_i^2 - 1)$$

where: $A_i = dx_{(i)}/dX_{(i)}$ – relative stretch in the direction of i axis, $dx_{(i)}$, $dX_{(i)}$ – denote the current and initial length of infinitesimal line element, aligned with i -axis before deformation.

Strain components, which characterize the change of angle between two perpendicular lines, are defined as written below:

$$(2.2) \quad E_{ij} = \frac{1}{2}A_iA_j \sin \Gamma_{ij}$$

where: Γ_{ij} – change of angle between two different axes i, j .

When the deformation is given by the deformation gradient \mathbf{F} , the strain tensor can be obtained using the following formula:

$$(2.3) \quad 2\mathbf{E} = \mathbf{F}^T \mathbf{F} - \mathbf{I}$$

where: \mathbf{I} – unit tensor.

Two stress tensors may be used to describe the stress state. The first Piola–Kirchhoff stress tensor \mathbf{T} , is aligned with the directions of the initial tangent base vectors in the undeformed state and the second Piola–Kirchhoff stress tensor $\mathbf{\Pi}$, referred to axes aligned with the tangent base vectors in the deformed state.

Both tensors comply with the relation:

$$(2.4)_1 \quad \mathbf{\Pi} = \mathbf{F}^{-1} \mathbf{T}$$

and the following relation with the Cauchy's stress tensor $\boldsymbol{\sigma}$:

$$(2.4)_2 \quad \boldsymbol{\sigma} = J^{-1} \mathbf{F} \mathbf{\Pi} \mathbf{F}^T.$$

2.2. Constitutive equations

The linear constitutive equations for various cellular structures may be found in many works by KRAYNIK [2], JANUS-MICHALSKA [6], WANG, MCDOWELL [15], where the stiffness matrix components are expressed as functions of microstructural geometric and material parameters. These constitutive relations can be extended to the large displacements and small strain case by rewriting them as a relationship between the Lagrangean strain tensor and the second Piola–Kirchhoff stress tensor [10, 11]. For the case of small strains, after application of expansion into Taylor series, if the first-order expression is taken into account, the relation can be written as follows:

$$(2.5) \quad \mathbf{\Pi}(\mathbf{E}) = \left. \frac{\partial \mathbf{\Pi}}{\partial \mathbf{E}} \right|_{\mathbf{E}=0} : \mathbf{E} = {}^0\mathbf{S} : \mathbf{E}$$

where: ${}^0\mathbf{S}$ – initial elasticity tensor (initial tangent operator).

Fully nonlinear range must be established in terms of a hyperelastic strain energy potential what will be the subject of further investigations.

3. Micromechanical analysis

In the present study, the strain stress relation for cellular materials will be given, based on studies of mechanical response on a microscale. On microscale only, the brief outline of micromechanical analysis, which was the subject of the previous works by JANUS-MICHALSKA [6] is given.

Fundamental study of deformation on a micro-scale yields the explanation of macroscopic behavior of such structured bodies. The effective properties are then used to determine the response of structural elements on a macro-scale and emerge naturally as a consequence of micro-macro transition, without depending on specific physical measurements. Such a derivation is typical for micromechanical modeling [13].

In micromechanics it is assumed that essential macroscopic features of mechanical behavior can be inferred from the deformation response of a representative volume element.

The concept is applied to chosen cellular materials with different structures exhibiting regular cell arrangement. For the sake of simplicity, two-dimensional planar model is proposed to be sufficient for planar deformation analysis, but without losing the generality, the framework is also valid for a 3D analysis.

3.1. Cellular microstructure

Cellular materials reveal different anisotropic properties due to variations in material structure topology. Materials with repetitive microstructure can be modeled by idealized, regularly repeating pattern of unit cells. A skeleton of a cell is modeled as elastic beam structure with stiff joints. The following planar cellular structures are analyzed: a) square cell structure, b) ‘honeycomb’ structure, c) equilateral triangular structure. Each structure may be represented by a unit cell, in part filled by skeleton with i half-struts \mathbf{b}_i^0 of length $|\mathbf{b}_i^0| = L_{0-i}/2$ measured from vertex 0 (node) to point i , A_i faces perpendicular to struts i and occupying volume V . Figure 1 shows material structures mentioned above and their representative unit cells.

Linear elastic brittle skeleton material with the following material data is adopted: σ_f^s – the modulus of rupture, E_s – Young’s modulus.

The considered structures in real cellular materials can be microdimensional and material parameters on microscale are not identical with the material parameters of material considered as a bulk. In such a case, the tension test is performed on individual ligament sample in order to determine experimentally the ligament Young modulus and rupture modulus. This approach is applied for foams and has been presented by BEECHEM and LAFDI [26].

Cellular structures of greater dimensions can be also described by the presented micromechanical approach. In this case, material parameters are similar as for bulk material.

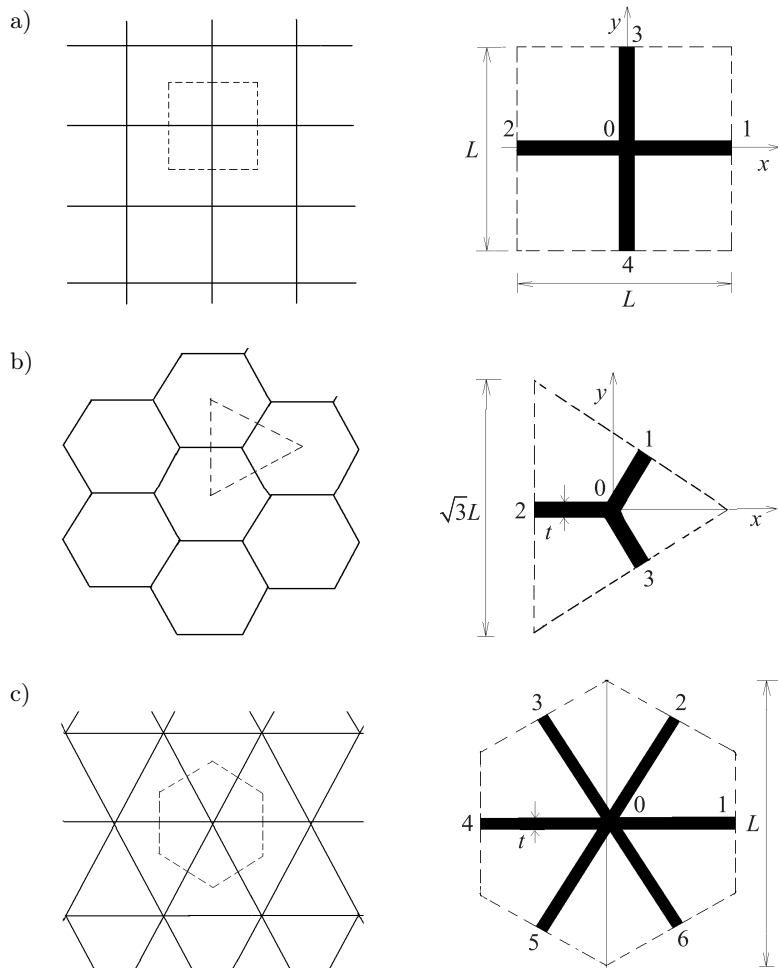


Fig. 1. Regular planar cellular structures, their material symmetries and representative unit cells. a) Square cell structure, square unit cell; tetragonal material symmetry. b) ‘Honeycomb’ structure, triangular unit cell; transversely isotropic material symmetry. c) Equilateral triangular structure, hexagonal unit cell; transversely isotropic material symmetry.

3.2. Microstructural deformation

A framework of micromechanical modeling begins with analysis of uniform deformation on macro-scale, defined in micromechanics by gradient of deformation as follows [13]:

$$(3.1)_1 \quad \mathbf{F} = \frac{1}{V} \int_{\partial V} (\mathbf{x} \otimes \mathbf{N}) dA$$

where: \mathbf{x} denote current position vector, \mathbf{N} – unit normal to the cell boundary in reference configuration.

For the given microstructures with beam solid skeleton, the formula is equivalent to:

$$(3.1)_2 \quad \mathbf{F} = \frac{1}{V} \sum_{A_i} (\mathbf{x}_i \otimes \mathbf{N}_i) dA_i$$

where: $\mathbf{x}_i = \mathbf{X}_i + \Delta_i$ for midpoints $i = 1, 2 \dots n$, Δ_i – midpoint displacement, A_i – face perpendicular to i strut, $\mathbf{N}_i = \mathbf{b}_i^0 / |\mathbf{b}_i^0|$.

Detailed description of deformation is given in [6] and repeated in the Appendix. The example of uniform deformation is presented in Fig. 2. Relevant midpoint displacements can be expressed as a sum of relative displacements of the beam midpoints with respect to the junction point (vertex) and vertex rigid motion as written below [6]:

$$(3.1) \quad \Delta_i = \Delta_{i-0} + \Delta_0 + \boldsymbol{\psi} \times \mathbf{b}_0$$

where: Δ_0 – translational component of rigid motion, $\boldsymbol{\psi}$ – rotation.

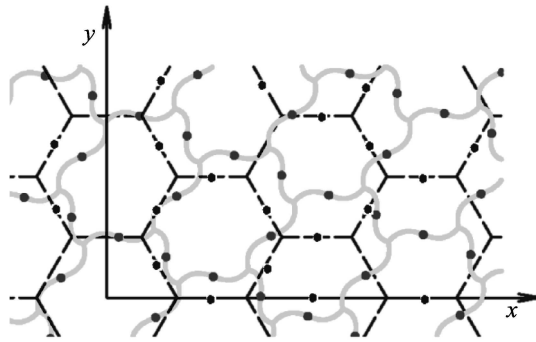


FIG. 2. Displacements in uniform deformation.

It is important to notice that only relative components produce forces in microstructure. The most important fact is that the large displacements on the macroscopic level usually result in smaller deformations of the individual struts constituting the skeleton. Nonlinear response in macroscale stems from the re-orientation of struts in the microstructure.

For regular periodic infinite structures in homogeneous deformation modes, the interaction between neighbouring RVE is represented only by forces, since moments vanish due to affinity of nodal displacements (Appendix 1a). The affinity of nodal displacements observed in Fig. 2 was presented and described in earlier works by WARREN and KRAYNIK [1, 2] and confirmed in experiments by microtomography methods. This justifies application of Cauchy to Cauchy averaging rules for micro-macro transition.

To represent cellular material, classical Cauchy continuum theory has been applied. This theory does not take into account size effects or edge effects typical for micromorphic continua [25]. For comparison of theoretical predictions with experiments, macroscopic sample size d must fulfill condition $d \gg L$ (in practice, condition $d > 10L$ is sufficient to obtain reasonable results [25]). To avoid this assumption and simplification, generalized continuum theory should be adopted for analysis [20, 21]. The example of application of micropolar Cosserat continuum for two-scale modeling of cellular material can be found in works by JÄNICKE, DIEBELS, SEHLHORST, DÜRSTER [21].

3.3. Mechanical model of cellular skeleton structure

Typical skeleton of cellular microstructure consists of thick beams, which may be described by Timoshenko beam model. The methods of structural mechanics are used to analyze this skeleton structure. Resultant forces, for the sets of midpoint displacements related to uniform deformation, can be obtained using the FEM code.

The idea of micro-macro transition applied here is presented in [6] and repeated in the Appendix.

3.4. Initial stiffness matrix

The model adopted here is based on equivalence of the strain potential for the discrete structure and the strain potential of an effective continuum. It refers to averaging of the strain energy density [13] as written below:

$$(3.2) \quad \Phi_E = \langle {}^s\Phi_E \rangle_V = \frac{1}{V} \int_{V_s} ({}^s\Phi_E) dV_s$$

where: $\langle \rangle_V$ stands for the volumetric average in skeleton s taken over V , V – volume of unit cell, V_s – volume of skeleton in unit cell.

For simplicity it is convenient to express strains, stresses and stiffness matrix in terms of a 6-D space with Kelvin notation, where plane strain tensor is represented by vector $({}^I\varepsilon)$, $I = 1, 2, 3$ and stiffness tensor representation for a 2D problem is S_{IJ} matrix, 3×3 .

The following stiffness matrix components for equivalent continuum can be obtained using the following formula [11]:

$$(3.3) \quad {}^0S_{IJ} = \frac{1}{V} \left(\frac{\partial^2 \left(\int_{V_s} {}^s\Phi_E dV_s \right)}{\partial({}^I\varepsilon) \partial({}^J\varepsilon)} \right).$$

Stiffness matrix components are given by analytical formulae – either in dependence on microstructural geometric and skeleton material para-

meters or obtained as a result of numerical procedure by the FEM code (Appendix).

3.5. Evaluation of elastic range

For anisotropic solids with linear stress-strain relation on a macroscale, an energy-based approach to limit conditions was proposed by M.M. MEHRABADI and C. COWIN [12], and RYCHLEWSKI [16]. The idea is based on the orthogonal energy elastic stress states concept, thus making possible the additive decomposition of the elastic energy density, stored in an anisotropic body. The criterion is formulated as a sum of weighted energy densities, stored in eigenstates as written below:

$$(3.4) \quad \sum_{\alpha=I}^{III} \frac{\alpha \Phi_E}{\alpha \Phi_E^{cr}} = 1$$

where: $\alpha \Phi_E^{cr}$ – critical energy density stored in an α eigenstate of stiffness matrix ${}^0\mathbf{S}$, $\alpha = I, II, III$, for a 2D problem.

Geometric nonlinear energy density stored in alfa eigenstate for arbitrarily given strain state is given by formula:

$$(3.5) \quad \alpha \Phi_E = \lambda_\alpha (\alpha E)^2$$

where: λ_α – α eigenvalue of stiffness matrix ${}^0\mathbf{S}$, $\alpha \mathbf{E}$ – α strain eigenstate, $\alpha E = |\alpha \mathbf{E}| = \sqrt{\alpha \mathbf{E} \cdot \alpha \mathbf{E}}$.

Critical energy density is given by formula:

$$(3.6) \quad \alpha \Phi_E^{cr} = \lambda_\alpha (\alpha E^{cr})^2$$

where: $\alpha \mathbf{E}^{cr} = \alpha k \alpha \tilde{\mathbf{E}}$, αk – scalar multiplier of unit eigenstrain, $\alpha \tilde{\mathbf{E}}$ – unit eigenstrain.

Eigenvalues λ_α and eigenstates $\alpha \tilde{\mathbf{E}}$ are given by analytical formulae in dependence on microstructural geometric and skeleton material parameters or can be obtained as a result of numerical procedure (Appendix).

Since the energy refers to linear elastic work of skeleton structure, critical energy densities stored in subsequent eigenstates are the same as in a linear case, although on macroscale it gives a geometrically nonlinear effect.

The detailed algorithm to calculate critical energies using micro-macro transition has been described in previous works on cellular materials [5, 6].

4. Homogeneous deformations

4.1. Loading cases

The presented theory is limited to problems of homogeneous states of deformation.

The loadings are chosen in such a way that they correspond to typical experiments.

The effective stress-strain behavior is analyzed under the following three types of loading:

- A) uniaxial load in tensile and compressive range $\sigma_x \neq 0$, $\sigma_y = 0$, $\tau_{xy} = 0$;
- B) biaxial load in tensile and compressive range $\sigma_x = \sigma_y = \sigma_1 \neq 0$, $\tau_{xy} = 0$;
- C) simple shearing deformation $\sigma_x = 0$, $\sigma_y \neq 0$, $\tau_{xy} \neq 0$,

where σ_x , σ_y , τ_{xy} denote components of Cauchy stress.

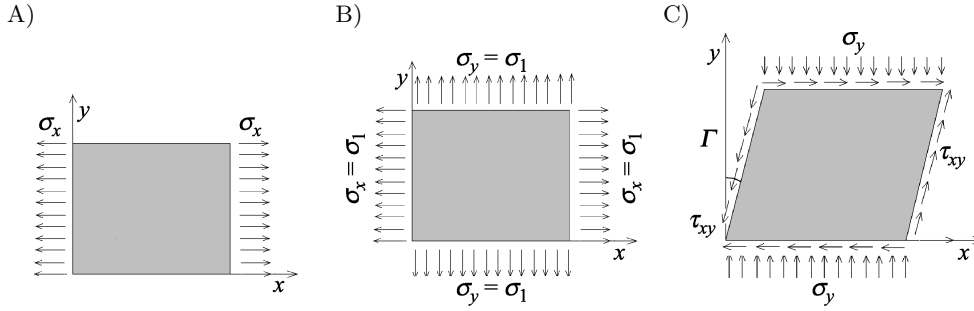


FIG. 3. Stress states corresponding to applied stretches loadings.

The deformation gradients for subsequent types of loadings are as follows:

$$(4.1) \quad {}^A\mathbf{F} = \begin{bmatrix} {}^A\Lambda_x & 0 \\ 0 & {}^A\Lambda_y \end{bmatrix}, \quad {}^B\mathbf{F} = \begin{bmatrix} {}^B\Lambda_x & 0 \\ 0 & {}^B\Lambda_y \end{bmatrix}, \quad {}^C\mathbf{F} = \begin{bmatrix} 1 & \Gamma \\ 0 & 1 \end{bmatrix},$$

where relative stretches fulfilling the stress conditions comply with the following relations:

$$(4.2) \quad {}^A\Lambda_y = \sqrt{\frac{S_{12} + S_{22} - S_{12}({}^A\Lambda_x)^2}{S_{22}}},$$

$${}^B\Lambda_y = \sqrt{\frac{S_{22} - S_{11} + (S_{11} - S_{12})({}^B\Lambda_x)^2}{S_{22} - S_{12}}},$$

where: S_{IJ} – stiffness matrix components in Kelvin's notation of the considered material with given microstructure.

4.2. Cellular material structures and skeleton material

Cellular materials of all presented types are considered. Type of microstructure is determined by topology of structural nodes. Basic geometric parameters L_{0-i} , t , determine the beam slenderness, which influences microstructural response due to resistance to axial and bending deformations. Cell orientation different than that given in Fig. 2 may present an interesting case [17]. Skeleton material parameters are specified separately, as they decide only on the magnitude of elastic range.

Numerical tests are carried out for a variety of combinations of geometric and material parameters. Results for chosen examples are presented for structures specified in Table 1. The structure a) is tested for two types of orientation as given in Fig. 4.

Table 1. Specification of microstructures.

Type	Geometric parameters of skeleton [mm]	Skeleton material parameters
a1)	$L_{01} = L_{02} = L_{03} = L_{04} = 20, t = 2.0$	$E_S = 2 \text{ GPa}, \nu_S = 0.33, \sigma_f^s = 60 \text{ MPa}$
a2)	$L_{01} = L_{02} = L_{03} = L_{04} = 20, t = 2.0, \beta = 45^{\circ 0}$	$E_S = 2 \text{ GPa}, \nu_S = 0.33, \sigma_f^s = 60 \text{ MPa}$
b)	$L_{01} = L_{02} = L_{03} = L_{04} = L_{05} = L_{06} = 20, t = 2.0$	$E_S = 2 \text{ GPa}, \nu_S = 0.33, \sigma_f^s = 60 \text{ MPa}$
c)	$L_{01} = L_{02} = L_{03} = 20, t = 2.0$	$E_S = 2 \text{ GPa}, \nu_S = 0.33, \sigma_f^s = 60 \text{ MPa}$

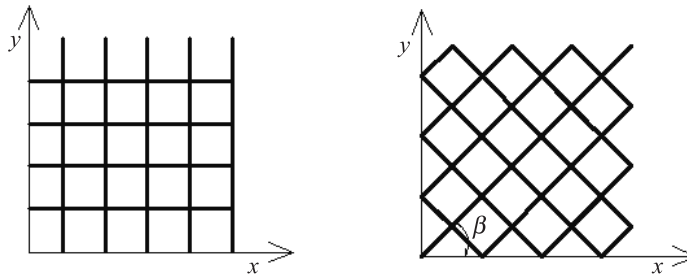


FIG. 4. Orientation of microstructure with respect to global coordinate axes giving structures a1) and a2).

Elastic range depends on skeleton material parameters and type of microstructure. Material parameters are chosen in such a way that the magnitude of maximum strains is not so small as infinitesimal strains and allows to observe the nonlinear path.

4.3. Results

Plots of Cauchy's stress versus relative stretch are presented for the load case A) in Fig. 5 as the result of numerical analysis performed in MATHCAD code. These plots are compared with results of linear analysis shown by in dashed line.

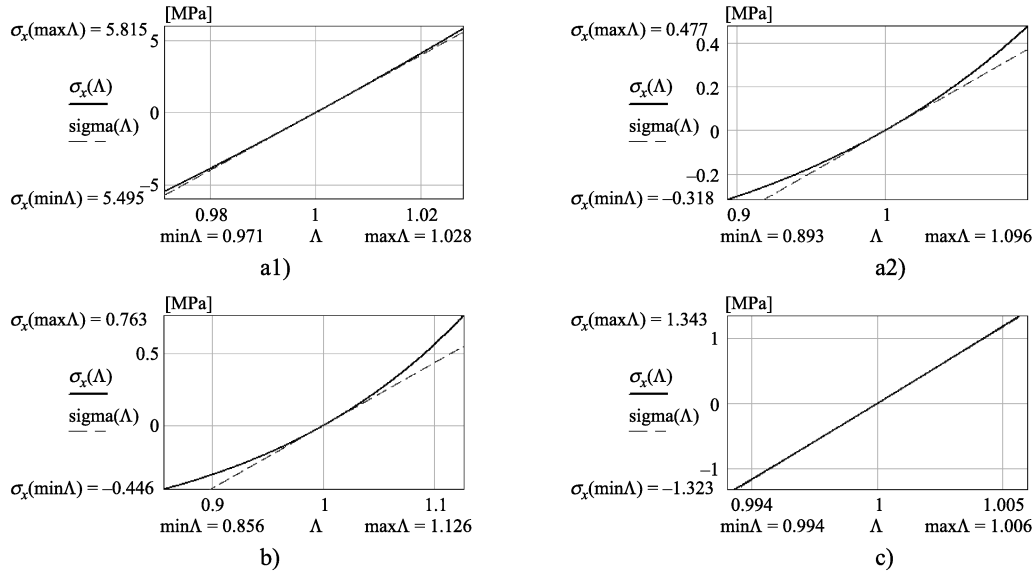


FIG. 5. Uniaxial tensile and compressive Cauchy stress σ_x versus the applied stretch Λ , for materials exhibiting the specified microstructures.

We may observe that the value of maximum tensile load differs from the absolute value of compressive load, resulting in material dissymmetry in tension-compression. The effect depends on the type of microstructure and its orientation with respect to the direction of load. Structures b) and c) are isotropic in plane, so the properties are independent of orientation. Generally, for stiff structures such as a1) and c), for which deformation response results in domination of axial forces in microstructure, the difference between geometric non-linearity and linear behavior is not significant. For compliant structures such as a2), b) for which bending of microstructural beams dominates, the dissymmetry in tension-compression is observed. Tests of the variety of combinations of geometric parameters indicates that for slender beam structures, this nonlinear effect is greater than that for thick ones for all types of microstructures.

For load case B) and materials of specified microstructures, the results are presented in Fig. 6.

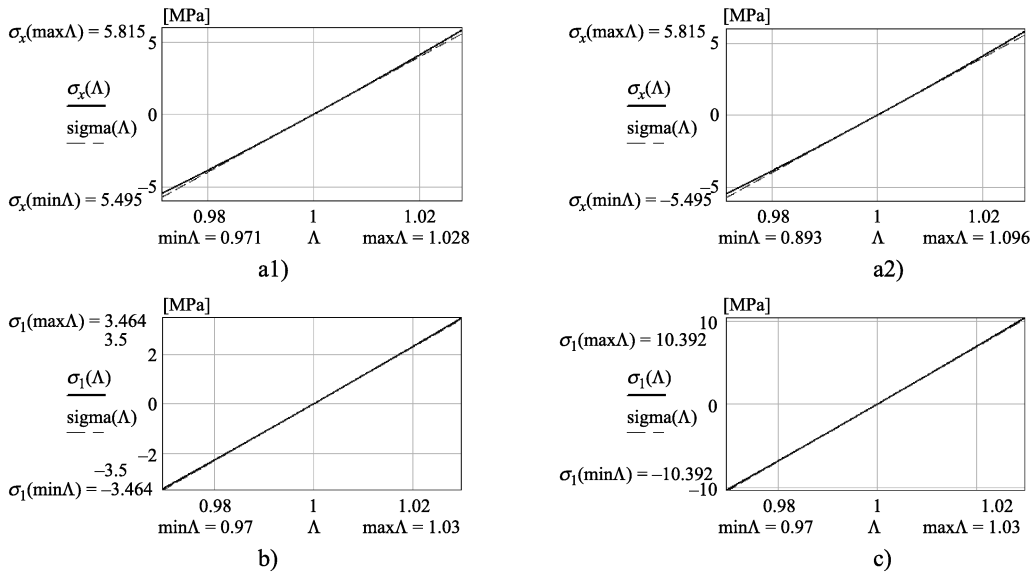


FIG. 6. Biaxial tensile and compressive Cauchy stress σ_1 versus the applied stretch Λ , for materials of specified microstructures.

Biaxial load results in axial microstructural response for structures a1), a2), b) and c) leading to a nearly linear behavior. It is visible that material response depends on the state of strains. This property is generally exhibited by stiffer response to biaxial load than to uniaxial ones.

Simple shearing deformation is obtained by applying shearing stress τ and normal compressive stress σ_Y . Nonlinear path for shearing stress versus shear angle is compared with linear predictions (dashed line) at the left of Fig. 7. A variety of behaviors is observed. The difference can be so great that linear analysis is not acceptable [structures a1), b)].

At the right of Fig. 7 a comparison of nonlinear paths for shearing stress with normal stress is presented. Anisotropic cellular material properties may result in various ratios of maximum values of these stresses.

4.4. Comparison of theoretical predictions with FEM solutions

The results shown in Figs. 5–7 are obtained with the use of the derived macroscopic, hyperelastic constitutive relation (2.5), with the limit of elasticity specified by (3.5). These predictions are now compared with numerical results for the corresponding beam structures mentioned in Sec. 3.3, under specified types of loadings with appropriate boundary conditions. These results are obtained using FEM code (ABAQUS). Structures are discretized by Timoshenko beam element, 36 elements per unit cell. For such a comparison, the most inter-

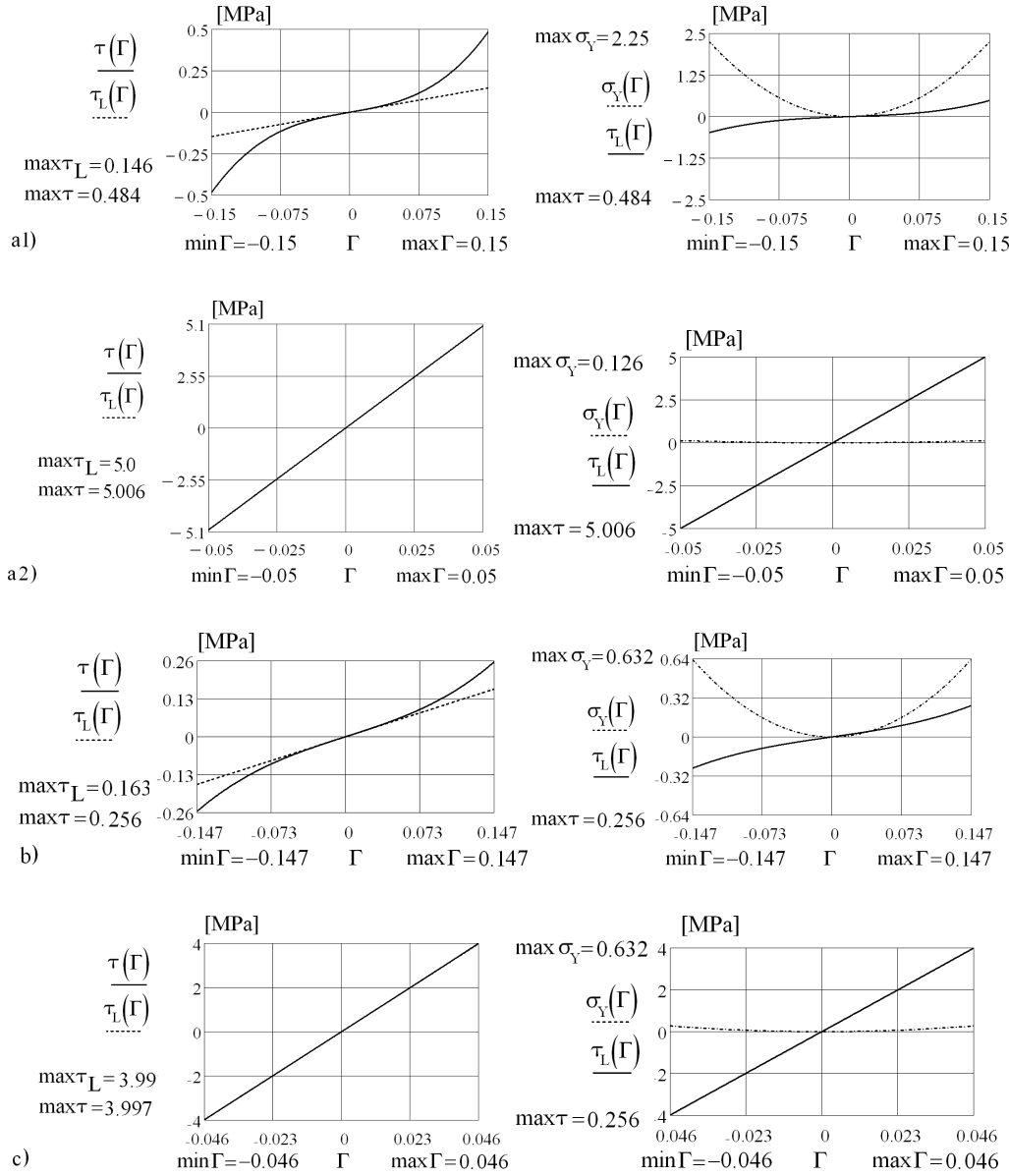
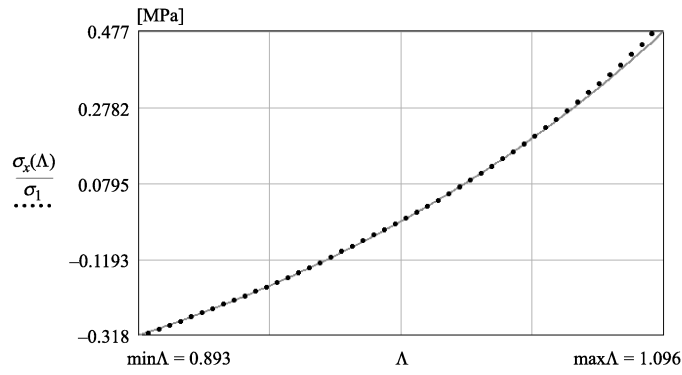


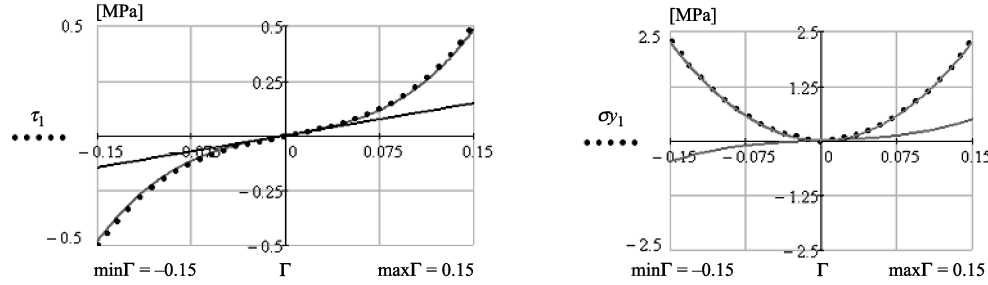
FIG. 7. Tangent and normal Cauchy stress versus the shearing angle for materials of specified microstructures.

esting are examples that reveal the difference between the nonlinear and linear behaviour.

Two chosen examples are presented in Fig. 8. Dotted line denote numerical nonlinear path. They show very good agreement of both methods.



Uniaxial tension, structure a2)



Simple shearing, structure a1)

FIG. 8. Comparison of theoretical predictions with numerical results for chosen examples.

5. Conclusions

This paper presents an application of constitutive equation for the hyperelastic cellular material exhibiting arbitrary symmetry. Almost every cellular material reveals nonlinear behavior in elastic range. For certain skeleton structures a linear analysis may be unacceptable, since the difference between linear and nonlinear behaviors is significant. The aim of this work is to prove that hyperelasticity of cellular solid stems from reorientation of struts, originating in rigid motion of structural nodes.

First-order FE^2 approach [19] is used to identify the microscopic deformation modes and the stress response of the skeleton. FEM analysis performed for Timoshenko beams is geometrically nonlinear (assumption of material linearity of skeleton material is adopted for simplicity and concentration upon geometric effects only). Detailed studies of numerical solution of the considered types of structures show that the main reason of nonlinearity lies in reorientation and other geometric effects are negligibly small. Structural topology and structural element stiffnesses influence the nonlinear path. Type of skeleton material and

type of microstructure determine the elastic range by the ratio σ_f^s/E_s . The non-linear effect depends also on the type of loading. The analytical and numerical strain-stress relations for cellular materials based on studies of mechanical response on a microscale constitute the objective of the present study. The theoretical model based on micromechanics requires experimental verification before application.

The work presented applies the first order homogenization technique. The alternative approach is based on formulation of consistent stiffness matrix [22–24]. This formulation gives direct evaluation of micro-macro transition and allows to model the mechanical response at large deformations.

Appendix A. Micro-macro transition

a) Kinematics

The essential feature of uniform deformation of solids with repetitive microstructure is the node displacement affinity. The individual beams deform antisymmetrically about their midpoints, so there is no resultant moment across the section at the beam midpoints. An example of such deformation is shown in the figure below:

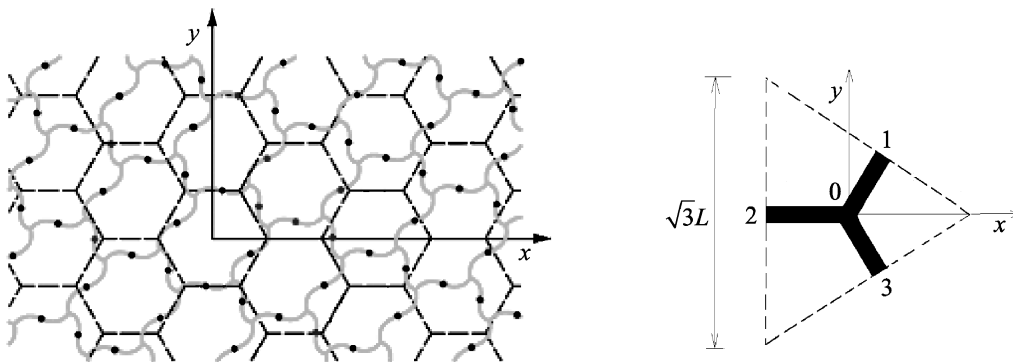


FIG. 9. The example of uniform deformation.

The kinematics of the unit cell is described by the relative displacements of the beam midpoints $i = 1, 2, \dots, n$, with respect to a rigid motion of the junction point (vertex 0). This rigid motion is described by the translation component Δ_0 and spatial rotation ψ . As a result, relative midpoint displacement with respect to node is given by the following formula:

$$(A.1) \quad \Delta_{i-0} = \Delta_i - \Delta_0 - \psi \times \mathbf{b}_0, \quad i = 1, \dots, n;$$

only this relative deformation produces forces in microstructure skeleton.

The uniform axial deformation ε_α in the α direction $\alpha = x, y$, results in the following midpoints displacements:

$$(A.2) \quad \Delta_i(\varepsilon_\alpha) = \varepsilon_\alpha \cdot (\mathbf{b}_i^0 \cdot \mathbf{e}_\alpha) \mathbf{e}_\alpha \quad i = 1, \dots, n.$$

For pure shearing deformation in the $\alpha\beta$ plane $\alpha \neq \beta$, the displacements are given as follows:

$$(A.3) \quad \Delta_i(\gamma_{\alpha\beta}/2) = (\gamma_{\alpha\beta}/2) \cdot ((\mathbf{b}_i^0 \cdot \mathbf{e}_\alpha) \mathbf{e}_\beta + (\mathbf{b}_i^0 \cdot \mathbf{e}_\beta) \mathbf{e}_\alpha), \quad i = 1, \dots, n,$$

where: \mathbf{e}_α – unit vector in α direction.

The location and rotation of the junction point is determined by cell equilibrium:

$$(A.4) \quad \sum_{i=1}^n \mathbf{F}_i = 0, \quad \sum_{i=1}^n \mathbf{F}_i \times \mathbf{b}_i^0 = 0.$$

Relative displacements may be represented by the components normal and tangent to the individual strut direction:

$$(A.5) \quad \Delta_{0-i} = \Delta_{0-i,n} + \Delta_{0-i,\tau}.$$

b) Displacement-force relations

Timoshenko beam model is adopted as the most appropriate model for short beams of the typical microstructure skeleton. The elastic behaviour of cantilever beam subject to axial and transverse loads is known from classical solutions.

For axial load F_{in} and transversal load $F_{i\tau}$, applied at the end of cantilevered beam, its free end axial displacement $\Delta_{i-0,n}$ and transversal displacement $\Delta_{i-0,\tau}$ may be described by linear relations with respect to the fixed end:

$$(A.6) \quad \Delta_{0-i,n} = F_{in} c_{in}, \quad \Delta_{0-i,\tau} = F_{i\tau} c_{i\tau},$$

where: c_{in} is defined as beam axial elastic compliance of strut i , $c_{i\tau}$ is defined as bending elastic compliance of strut i having the length $L_{0-i}/2$.

For a uniform beam cross-section, the solutions are as follows:

$$(A.7) \quad c_{in} = \frac{L_{0-i}}{2E_s A}, \quad c_{i\tau} = \frac{L_{0-i}^3}{24E_s J} + \frac{L_{0-i}}{2G_s A_\tau},$$

where: A – cross-sectional area, E_s , G_s – Young's and shear modulus for the skeleton material.

Axial and bending stiffnesses of beams are given by reciprocals of compliances:

$$(A.8) \quad s_{in} = (c_{in})^{-1}, \quad s_{i\tau} = (c_{i\tau})^{-1}.$$

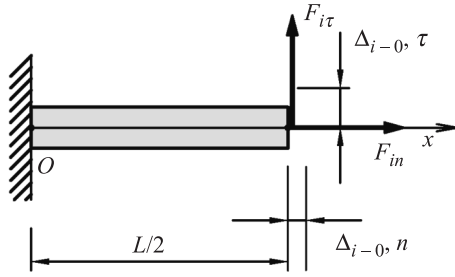


FIG. 10. Cantilevered beam representing microstructural element.

When the stiffnesses are determined, one may calculate the normal and transversal forces as functions of unknown nodal rigid motions using the force-displacement relations. The displacement and rotation components may be obtained from equilibrium equations (A.4). The solution supplies full description of the deformation mechanism.

c) Equivalent continuum based on averaging of the strain potential

The approach adopted here is based on equivalence of the strain potential for a discrete structure and the strain potential of an effective continuum. It refers to averaging the strain energy density [11] as written below:

$$(A.9) \quad \Phi_E = \langle {}^s\Phi_E \rangle_V = \frac{1}{V} \int_{V_s} ({}^s\Phi_E) dV_s.$$

Strain potential of beam skeleton in linear case may be obtained using the following formula [18]:

$$(A.10) \quad U = \int_{V_s} ({}^s\Phi_E) dV_s \\ = \sum_{i=1}^3 \left(\int_0^{l_i} \frac{(F_{ni})^2 d\xi_i}{2E_s A_s} + \mu \int_0^{l_i} \frac{(F_{\tau i})^2 d\xi_i}{2G_s A_s} + \int_0^{l_i} \frac{(F_{\tau i}(l_i - \xi_i))^2 d\xi_i}{2E_s J} \right)$$

where: E_s , G_s – Young's and shear modulus for the skeleton material, A_s , J – beam cross-sectional area and moment of inertia, μ – energy cross-sectional coefficient (for rectangular cross-section $\mu = 1.2$).

This strain potential (A.6) obtained as a function of subsequent uniform deformations is used for determination of initial stiffness matrix components.

Appendix B. Macroscopic material properties for cellular materials of the given structures

a) Material of square cubic symmetry – square cell structure

$${}^0\mathbf{S} = \begin{bmatrix} \frac{E_s t}{L} & 0 & 0 \\ 0 & \frac{E_s t}{L} & 0 \\ 0 & 0 & \frac{E_s t^3}{L^3} \end{bmatrix},$$

$$\begin{aligned} \lambda_I &= \frac{E_s t}{L}, & \lambda_{II} &= \frac{E_s t}{L}, & \lambda_{III} &= \frac{E_s t^3}{L^3}, \\ {}^I\tilde{\mathbf{E}} &= (1, 1, 0), & {}^{II}\tilde{\mathbf{E}} &= (1, -1, 0), & {}^{III}\tilde{\mathbf{E}} &= (0, 0, 1), \\ k_I &= \frac{R_e}{E_s}, & k_{II} &= \frac{R_e}{E_s}, & k_{III} &= \frac{R_e \sqrt{2} L}{E_s 3t}. \end{aligned}$$

b) Isotropic material – honeycomb structure

$${}^0\mathbf{S} = \begin{bmatrix} \frac{\sqrt{3}E_s t (L^2 + 3t^2)}{6L (L^2 + t^2)} & \frac{\sqrt{3}E_s t (L^2 - t^2)}{6L (L^2 + t^2)} & 0 \\ \frac{\sqrt{3}E_s t (L^2 - t^2)}{6L (L^2 + t^2)} & \frac{\sqrt{3}E_s t (L^2 + 3t^2)}{6L (L^2 + t^2)} & 0 \\ 0 & 0 & \frac{\sqrt{3}E_s t^3}{3L (L^2 + t^2)} \end{bmatrix},$$

$$\begin{aligned} \lambda_I &= \frac{\sqrt{3} E_s t}{3 L}, & \lambda_{II} &= \lambda_{III} = \frac{2\sqrt{3}}{3} \frac{E_s t^3}{L(2L^2 + t^2)}, \\ {}^I\tilde{\mathbf{E}} &= (1, 1, 0), & {}^{II}\tilde{\mathbf{E}} &= (1, -1, 0), & {}^{III}\tilde{\mathbf{E}} &= (0, 0, 1), \\ k_I &= \frac{R_e}{E_s}, & k_{II} &= \frac{R_e}{E_s} \frac{2(2L^2 + t^2)}{(2L^2 + 2t^2 + 3\sqrt{3}tL)}, & k_{III} &= \frac{R_e \sqrt{2}(L^2 + t^2)}{E_s (3L + t)t}. \end{aligned}$$

c) Isotropic material – equilateral triangular cell structure

$${}^0\mathbf{S} = \begin{bmatrix} \frac{\sqrt{3}E_s t (3L^2 + 2t^2)}{4L^3} & \frac{\sqrt{3}E_s t (L^2 - t^2)}{4L^3} & 0 \\ \frac{\sqrt{3}E_s t (L^2 - t^2)}{4L^3} & \frac{\sqrt{3}E_s t (3L^2 + 2t^2)}{4L^3} & 0 \\ 0 & 0 & \frac{\sqrt{3}E_s t}{4L} \end{bmatrix},$$

$$\lambda_{\text{I}} = \frac{\sqrt{3} E_s t}{3 L}, \quad \lambda_{\text{II}} = \lambda_{\text{III}} = \frac{2\sqrt{3} E_s t^3}{3 L(L^2 + t^2)},$$

$${}^{\text{I}}\tilde{\mathbf{E}} = (1, 1, 0), \quad {}^{\text{II}}\tilde{\mathbf{E}} = (1, -1, 0), \quad {}^{\text{III}}\tilde{\mathbf{E}} = (0, 0, 1),$$

$$k_{\text{I}} = \frac{R_e}{E_s}, \quad k_{\text{II}} = \frac{R_e}{E_s} \frac{2L}{L + 3\sqrt{3}t}, \quad k_{\text{III}} = \frac{R_e \sqrt{3}L}{E_s 12t}.$$

References

1. W.E. WARREN, A.M. KRAYNIK, *The nonlinear elastic behaviour of open-cell foams*, Transactions of ASME, **58**, 375–381, June 1991.
2. W.E. WARREN, A.M. KRAYNIK, C.M. STONE, *A constitutive model for two-dimensional nonlinear elastic foams*, Journal of the Mechanics and Physics of Solids and Structures, **37**, 717–733, 1989.
3. Y. WANG, A.M. CUITIÑO, *Three-dimensional nonlinear open cell foams with large deformations*, Journals of the Mechanics and Physics of Solids, **48**, 961–988, 2000.
4. J. HOHE, W. BECKER, *Effective mechanical behavior of hyperelastic honeycombs and two-dimensional model foams at finite strain*, International Journal of Mechanical Sciences, **45**, 891–913, 2003.
5. M. JANUS-MICHALSKA, R.B. PEÇHERSKI, *Macroscopic properties of open-cell foams based on micromechanical modeling*, Technische Mechanik, Band 23, Heft 2-4, 221–231, 2003.
6. M. JANUS-MICHALSKA, *Effective models describing elastic behavior of cellular materials*, Archives of Metallurgy and Materials, **50**, 595–608, 2005.
7. P. KORDZIKOWSKI, M. JANUS-MICHALSKA, R. PEÇHERSKI, *Specification of energy-based criterion of elastic limit states for cellular materials*, Archives of Metallurgy and Materials, **50**, 621–634, 2005.
8. R.W. OGDEN [Ed.], *Nonlinear Elasticity with Application to Material Modeling*, Center of Excellence for Advanced Materials and Structures, Warsaw 2003.
9. V.V. NOVOZHILOV, *Foundations of the Nonlinear Theory of Elasticity*, Dover 1999 (translated from Russian first edition, 1948).
10. M.M. ATTARD, *Finite strain isotropic hyperelasticity*, Int. Jour. of Solids and Struct., **40**, 4353–4378, 2003.
11. A. CHISKIS, R. PARNES, *Linear stress-strain relations in nonlinear elasticity*, Acta Mechanica, **146**, 109–113, 2001.
12. M.M. MEHRABADI, C. COWIN, *Eigentensors of linear anisotropic elastic materials*, Q. J. Mech. Appl. Math., **43**, 15–41, 1990.
13. S. NEMAT-NASSER, M. HORI, *Micromechanics*. 2nd ed., Elsevier, North-Holland, Amsterdam 1999.
14. S. NEMAT-NASSER, *Averaging theorems in finite deformation plasticity*, Mechanics of Materials, **31**, 493–523, 1999.

15. A.J. WANG, D.L. MCDOWELL, *In-plane stiffness and yield strength of periodic metal honeycombs*, Journal of Eng. Materials and Technology, **126**, 137–156, 2004.
16. J. RYCHLEWSKI, *Unconventional approach to linear elasticity*, Archives of Mechanics, **47**, 149–171, 1995.
17. J. LELLEP, J. MAJAK, *On optimal orientation of nonlinear elastic orthotropic materials*, Structural Optimization, **14**, 116–120, 1997.
18. M. JANUS-MICHALSKA, *Micromechanical model of auxetic cellular materials*, Journal of Theoretical and Applied Mechanics, **47**, 4, 2009 .
19. F. FEYEL, J.L. CHABOCHE, *FE² multiscale approach for modelling the elastovisco-plastic behaviour of long fiber SiC/Ti composite materials*, Comp. Meth. Appl. Mech. Engng., **183**, 309–330, 2000.
20. S. FOREST, K. SAB, *Cosserat overall modeling of heterogeneous materials*, Mech. Res. Commun., **25**, 449–454, 1998.
21. R. JÄNICKE, S. DIEBELS, H.G. SEHLHORST, A. DÜRSTER, *Two-scale modelling of micromorphic continua*, Continuum Mech. Therm., **21**, 4, 297–315, 2009.
22. V.G. KOUZNETSOVA, W.A.M. BREKELMANS, F.P.T. BAAIJENS, *An approach to micro-macro modeling of heterogeneous materials*. Comp. Mech., **27**, 37–48, 2001.
23. V.G. KOUZNETSOVA, M. G. D. GEERS V. A. M. BREKELMANS, *Multi-scale constitutive modelling of heterogeneous materials with a gradient-enhanced computational homogenization scheme*, Int. J. Numer. Meth. Eng., **54**, 1235–1260, 2002.
24. C. MIEHE, J. SCHOTTE, J. SCHRÖDER, *Computational micro-macro transition and overall moduli in the analysis of polycrystals at large strains*, Comp. Mat. Science, **16**, 372–382, 1999.
25. C. TEKODLU, P.R. ONCK, *Size effects in the mechanical behaviour of cellular materials*, J. Mat. Sci., **40**, 5911–5917, 2005.
26. T. BEECHEM, K. LAFDI, *Novel high strength graphitic foams*, Carbon, **44**, 1548–1559, 2006.

Received January 22, 2010; revised version November 30, 2010.
